Developing an Outcome Measure With High Luminance for Optogenetics Treatment of Severe Retinal Degenerations and for Gene Therapy of Cone Diseases

Artur V. Cideciyan,[1] Alejandro J. Roman,[1] Samuel G. Jacobson,[1] Boyuan Yan,[2] Michele Pascolini,[3] Jason Charng,[1] Simone Pajaro,[3] and Sheila Nirenberg[2]

[1]Scheie Eye Institute, Perelman School of Medicine, University of Pennsylvania, Philadelphia, Pennsylvania, United States
[2]Department of Physiology and Biophysics, Weill Cornell Medical College, New York, New York, United States
[3]Nidek Technologies, Srl, Padova, Italy

Purpose. To present stimuli with varied sizes, colors, and patterns over a large range of luminance.

Methods. The filter bar used in scotopic MP1 was replaced with a custom slide-in tray that introduces light from an external projector driven by an additional computer. MP1 software was modified to provide retinal tracking information to the computer driving the projector. Retinal tracking performance was evaluated by imaging the system input and the output simultaneously with a high-speed video system. Spatial resolution was measured with achromatic and chromatic grating/background combinations over scotopic and photopic ranges.

Results. The range of retinal illuminance achievable by the modification was up to 6.8 log photopic Trolands (phot-Td); however, in the current work, only a lower range over −4 to +3 log phot-Td was tested in human subjects. Optical magnification was optimized for low-vision testing with gratings from 4.5 to 0.2 cyc/deg. In normal subjects, spatial resolution driven by rods, short wavelength-sensitive (S-) cones, and long/middle wavelength-sensitive (L/M-) cones was obtained by the choice of adapting conditions and wavelengths of grating and background. Data from a patient with blue cone monochromacy was used to confirm mediation.

Conclusions. The modified MP1 can be developed into an outcome measure for treatments in patients with severe retinal degeneration, very low vision, and abnormal eye movements such as those for whom treatment with optogenetics is planned, as well as for patients with cone disorders such as blue cone monochromacy for whom treatment with gene therapy is planned to improve L/M-cone function above a normal complement of rod and S-cone function.

Keywords: channelrhodopsin, optogenetics, outcome measures, retinal degeneration, low vision

Inherited retinal degenerations (IRDs) are a molecularly heterogenous group of diseases that cause progressive loss of photoreceptors and blindness.[1] There is currently only one Food and Drug Administration (FDA)-approved treatment for IRDs that involves the surgical implantation of an electronic stimulator chip in eyes with no photoreceptors or vision left.[2] Other treatment strategies at various stages of development include those that aim to substitute for lost neurons, arrest ongoing progression, improve visual function, or prevent the onset of the disease.[3] Optogenetics belongs to the first category, in which light-sensitive channels are introduced into nonphotoreceptor retinal cells.[4–10] An optogenetics clinical trial attempting to express channelrhodopsin with the use of intravitreally injected adeno-associated virus (AAV) vector in ganglion cells has recently started (NCT02556736, Clinicaltrials.org). Gene augmentation therapy belongs to the second and third categories, in which the wild-type gene is introduced into the affected retinal tissue.[11,12]

There is no single outcome measure that is appropriate for varied treatment approaches designed for different stages of diseases with vastly diverse underlying pathobiology. For optogenetics treatments in severely affected IRD eyes, currently available outcome measures will likely encounter at least four major obstacles. First, many of the light-sensitive channels available for optogenetics today are relatively insensitive to ambient light[13,14] and thus require additional technology that transforms ambient light from natural scenes to a high-illuminance version to be presented to the retina.[15–18] Second, there is a need for an encoding scheme that simulates the natural intraretinal processing in order to make a natural scene intelligible by activation of postreceptoral cells.[10,19] Third, eyes with low vision tend to have lost normal oculomotor control[20–22] and thus require eye tracking methods to allow presentation of high-luminance encoded patterns to a specific part of the retina reproducibly time after time. And finally, currently available AAV vectors from intravitreal injections have

TABLE. Subjects

No.	Age at Visit, Years	Sex	Eye	Mutation	Visual Acuity	Refraction	Previous Publication
Patients							
P1	13	F	LE	*CNGA3*-ACHM	20/125	+4.00	CHRD4313 in Zelinger et al. 2015
P2	18	M	RE	*CNGB3*-ACHM	20/150	−6.00	–
P3	24	M	LE	BCM	20/80	−9.25	P26 in Luo et al. 2015
P4	31	M	RE	BCM	20/125	−6.50	P10 in Luo et al. 2015
P5	66	M	RE	*RPGR*-XLRP	Light perception	−3.50	–
Normals							
N1	28	F	RE	Normal	20/16	+0.50	–
N2	31	M	LE	Normal	20/16	−1.50	–
N3	32	F	LE	Normal	20/16	Plano	–
N4	51	F	LE	Normal	20/16	−1.25	–
N5	52	M	LE	Normal	20/20	−3.25	–

produced an annular expression of channelrhodopsin in ganglion cells surrounding the fovea[23,24]; thus natural scenes need to be converted to an annular form to maximize the availability of information content.[25]

For gene augmentation therapy aimed at improving retinal function, it is important for outcome measures to be able to distinguish native visual function that exists before the treatment from the potential new function. This differentiation is especially challenging in cone disorders where normal rod function reserved for night vision can provide some level of daylight vision.[26-28] Currently available outcome measures such as visual acuity, perimetry, and flicker ERGs are not likely to distinguish the native rod function from small incremental cone-driven gains even though the latter may have very significant implications regarding evidence of biological effects in early clinical trials.

Here we modified the Nidek MP1 microperimeter (Nidek Technologies, Padova, Italy) in order to generate high-luminance chromatic stimulation under precise spatiotemporal control. We performed experiments evaluating spatial resolving properties driven by the rod, long/middle wavelength-sensitive (L/M-) cone, and short wavelength-sensitive (S-) cone systems near their respective increment thresholds in order to better understand subtle efficacy signals that are likely to result from early-stage therapies. Our results suggest that the modified MP1 may be a useful tool in developing relevant outcome measures for very low-vision patients undergoing optogenetics treatment and for patients with achromatopsia (ACHM) or blue cone monochromacy (BCM) undergoing gene augmentation treatment.

METHODS

Human Subjects

Patients with retinal degeneration ($n = 5$) and subjects with healthy vision ($n = 5$) participated in this study (Table). All subjects had complete clinical ocular examinations, including best-corrected visual acuity. All testing was performed with dilated pupils. The tenets of the Declaration of Helsinki were followed, and informed consent and assent were obtained from all patients. The research was approved by the institutional review board at the University of Pennsylvania.

Modification of the MP1S Microperimeter Hardware

In the standard MP1 system, optical paths of the retinal imaging and stimulation systems partially overlap. For the retinal imaging system, infrared illumination enters the dilated pupil, and the proportion reflected by the retina is imaged by a camera running at 25-Hz frame rate (Fig. 1A, red arrows). For the stimulation system, a second light path allows the subject to focus onto an internal liquid crystal display (LCD) screen that shows targets locked to a specific retinal location based on tracking of retinal features (Fig. 1A, blue arrows). The scotopic version of the MP1 instrument (MP1S) adds a filter holder rail placed between the final lens and the LCD screen (in addition to other software and hardware modifications) in order to allow for two-color microperimetry under dim backgrounds.[29,30] The modification used in the current work was designed to build further upon the MP1S and consisted of a custom-machined slide-in tray that inserted directly into the filter holder rail (Figs. 1A, 1B). The tray held an optical relay assembly and an external microprojector (DLP Lightcrafter with DLP3000 micromirror array; Texas Instruments, Dallas, TX, USA). The optical relay assembly consisted of two achromatic doublets ($L_1 = 47$-713 and $L_2 = 49$-292; Edmund Optics, Barrington, NJ, USA) and a front-surface mirror (M_1, Edmund Optics). Software control of 8-bit red, green, and blue (R, G, B) values provided >2 log units of dynamic range of the DLP output controllable digitally. In addition, there were slots (F_2 and F_4) for the introduction of absorptive neutral density (ND) filters (e.g., 65-822, Edmund Optics) to attenuate the light output by up to 9 log units. The scattered light from the internal LCD screen was blocked (X_1). A long-pass filter (F_1) was mounted in front of the camera to block scattered light from the projector reaching the detector. For future studies intending to use higher levels of output, a short-pass (<625 nm) filter ($F_3 = 84$-723, Edmund Optics) can be used to spectrally shape the light in order to avoid saturating the retinal imaging system.

Modification of the MP1S Microperimeter Software

The standard manufacturer's MP1 software (Ver. 1.7.8) tracks each frame of the video image compared to a reference image obtained at the start of each session; the tracking result is an estimate, approximately every 40 ms, of the shift in degrees in two orthogonal directions. This estimate is used to shift the location of the stimulus presentation such that the same retinal location can be repeatedly stimulated. The standard software contains an option to send all the tracking data to a log file. For the current project, the manufacturer modified the standard MP1 software such that the stream consisting of the time stamp, and x and y values of shifts and tracking success, was sent through a serial communication link (USB NMC-2.5m; FTDI Ltd., Glasgow, UK).
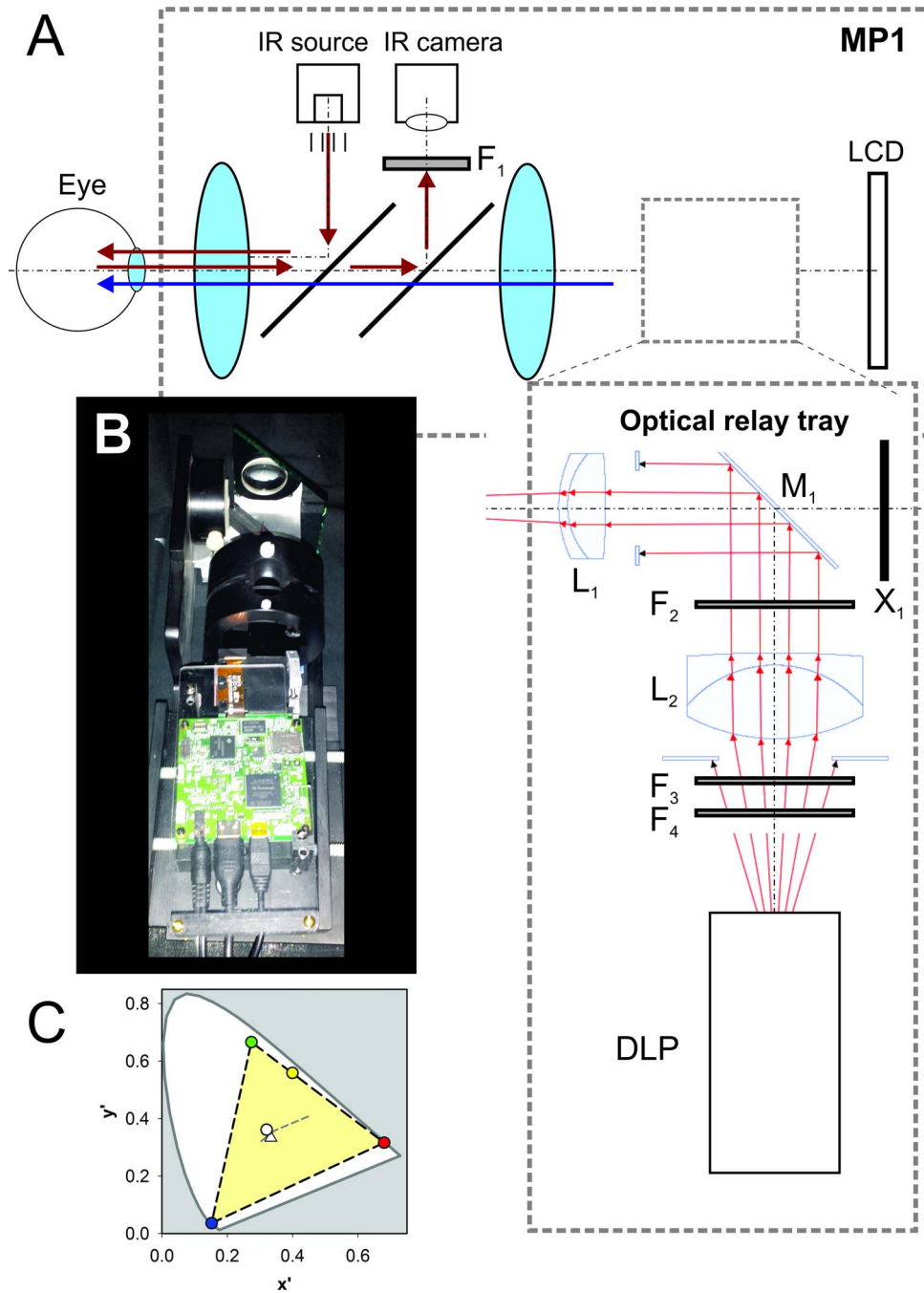
FIGURE 1. Modification of the MP1 microperimeter to optically couple an external DLP projector. (**A**) Schematic of the MP1 system and the light paths under the unmodified and modified conditions. The retina is illuminated with an infrared source and the reflected light from the retina is imaged with a camera (light path shown with *red arrows*). In addition, a stimulus shown on the internal LCD screen is imaged on the retina (light path shown with *blue arrow*). Modification adds F1 and the optical relay tray. F1 is a long-pass filter in front of the camera in order to minimize the stray light originating from the external DLP; this is relevant only when the modified MP1 is used under high-luminance conditions. The optical relay tray is introduced between the final lens and the LCD using the rail normally carrying the filters used for scotopic testing. The relay tray bends the light path 90° away from the LCD (front-surface mirror M_1) and focuses the DLP projector onto the retina along the stimulus path. Ray traces are shown with *red*. Two lenses, L_1 and L_2, are used to form a virtual image at the same plane as the LCD. Filters F_2, F_3, and F_4 spectrally shape and attenuate the DLP light output. X1 is an opaque cover to prevent stray light from the internal LCD from reaching the eye. (**B**) Photograph of the optical relay tray inserted into the MP1 scotopic filter slot. (**C**) Judd chromaticity diagram of the DLP light coupled to the modified MP1. *Red-, green-, blue-, yellow-,* and *white-filled circles* correspond to R, G, B settings of (255, 0, 0), (0, 255, 0), (0, 0, 255), (255, 255, 0), and (255, 255, 255), respectively. *Dashed lines* delineate the final system gamut (*light yellow area*) within the standard observer. *Triangle symbol* indicates the equal-energy white point in the diagram. *Gray dashed line* shows the position of several CIE standard illuminators.

External Computer and Software

A laptop computer (running Ubuntu 15.04 Linux) was connected to the DLP via HDMI (High-Definition Multimedia Interface) and USB ports and to the MP1 computer via a USB port acting as the serial communication link. The laptop was set up in a two-screen mode, and the second screen was defined as the projector connected through the HDMI port. Custom software was written (Java 8 SE; Oracle Corp, Redwood City, CA, USA) to read retinal tracking information obtained from the MP1 computer through one USB port and control the DLP through commands sent via another USB port. Three light-emitting diode (LED) illuminators (R = 624 nm, G = 526 nm, B = 454 nm) of the DLP were run with the default current setting of 633 mA. In theory, the LED illuminators can be run at up to 1.5 A each to increase illumination; however, that approach requires active cooling and was not used in the current work. Importantly, default settings of the DLP include a variety of color correction matrices such that specific changes to R, G, and B values do not necessarily correspond to equivalent changes in light output. These color correction matrices were all disabled for the current work.

Psychophysics Used in Feasibility Experiments

In the current work, feasibility experiments were performed to help design and develop outcome measures in the future based on detection and discrimination thresholds for specific conditions and specific interventions. All thresholds used forced-choice methods where the presentation of a 0.5-second-long stimulus was paired with a sound and the subject was asked to respond following the sound. In a small subset of experiments, the subject indicated whether the stimulus was detected. In the great majority of experiments, the task was to discriminate between two possible alternatives representing the diagonal direction of a flashed grating. In this two-alternative forced-choice (2AFC) paradigm, the subject pressed one of two buttons of a modified numeric keyboard depending on the perceived direction of the stimulus, and the software recorded the response. Appropriate for eventual outcome development for the clinic, there were 5 to 10 trials for each test condition depending on the difficulty of the task; full psychophysical functions were not performed. After each experiment, all data were downloaded and analyzed offline together with a reference retinal image obtained at the start of each session. The "threshold" was considered to correspond to the trial with the highest spatial frequency grating whose direction could be discriminated with no more than one incorrect answer.

Maximum Retinal Illuminance

The MP1 uses a Maxwellian illumination system where the retinal illuminance is the total power entering the dilated pupil divided by the retinal exposed area.[31] To calculate the maximum retinal illuminance achievable with the modified MP1 system using the external DLP as the illumination source, the power entering the pupil was estimated by first measuring the irradiance in air at 50 cm with a calibrated radiometer (IL1700; International Light, Peabody, MA, USA) and then multiplying this value by the area illuminated at that distance. The size of the DLP projector extent that is projectable onto the retina through the optical relay was nearly circular with a 32° diameter. Thus the total power of 6.77-mW white light entering the pupil corresponded to the estimated maximum retinal illuminance of ~0.1 mW.mm^{-2} for an emmetropic eye. For this maximum estimate, transmission losses through the cornea and lens were not considered since they are rarely quantifiable in patients.

The maximum achromatic light output was estimated to correspond to a photopic luminance of 6.3 log phot cd.m^{-2} (retinal illuminance of 6.8 log photopic Trolands [phot-Td]) and a scotopic luminance of 6.7 log scot cd.m^{-2} (7.1 log scotopic Trolands [scot-Td]). The gamut of stimulus chromaticities (x', y' Judd chromaticity coordinates[32,33]) that can be produced with the modified MP1 are shown in Figure 1C. For all of the feasibility experiments performed in the current work in human subjects, a 3 ND filter was always in the light path, substantially limiting the light output.

Achromatic and Chromatic Gratings

Feasibility experiments were performed in normal subjects and one BCM patient with stimuli consisting of unitary contrast grating patches superimposed on larger homogeneous background fields. The color and luminance of the background were varied to provide different levels of adaptation to photoreceptor systems. The color and peak luminance of the gratings were varied to provide different increments above the adapting backgrounds; the troughs of the gratings were equal to the background. The gratings were oriented along one of two diagonals 45° from vertical and had a sinusoidal spatial profile perpendicular to the orientation. A radially varying sigmoid-shaped envelope with a flat top was applied to smoothly blend the border of the grating into the background. The range of spatial frequencies available was 0.2 to 4.7 cyc/deg. Examples of achromatic (white on white, WonW) and chromatic (blue on yellow, BonY, and red on blue, RonB) gratings demonstrate their appearance (Fig. 2A).

The adapting background was on continuously, and gratings were flashed for 0.5 seconds following an auditory signal. In most experimental runs, the subject was asked to discriminate between the two directions of gratings by pressing one of two buttons in a 2AFC testing paradigm. For each combination of grating and background, spatial frequency was varied to estimate the highest spatial frequency that could be correctly discriminated by the subject. The choice for testing along the spatial frequency (as opposed to testing along the luminance/chromaticity) axis was based on our interest in finding a single combination of grating and background for future outcome development. Furthermore, in order to be able to perform the testing in a clinical setting quickly, a complete psychometric function was not used. Instead, between 5 and 10 trials were presented (depending on the difficulty of the discrimination task) at each spatial frequency, progressing from lower to higher spatial frequencies. The highest spatial frequency with zero or one incorrect was considered to be the discrimination threshold. If the subject reliably discriminated the finest spatial frequency (4.7 cyc/deg) available, the threshold was considered indeterminate. If the subject could not discriminate the coarsest spatial frequency (0.2 cyc/deg), the stimulus was presented without a grating (zero spatial frequency; a disc of peak intensity) in order to determine the detectability of the increment under those conditions.

The background was always 32° in diameter. Gratings of 11° diameter were presented nasal to the optic nerve centered at an eccentricity of 22° (Fig. 2A, inset). The fixation was to either four small squares brighter than background for scotopic conditions, or a single small square darker than the background for photopic conditions. The retinal illuminance in phot-Td was estimated for each stimulus condition using measured values of illuminance in photopic lux at 100 mm.[34] The retinal illuminance in scot-Td was similarly estimated from measures of scotopic lux. The retinal illuminance in S-cone Trolands (s-
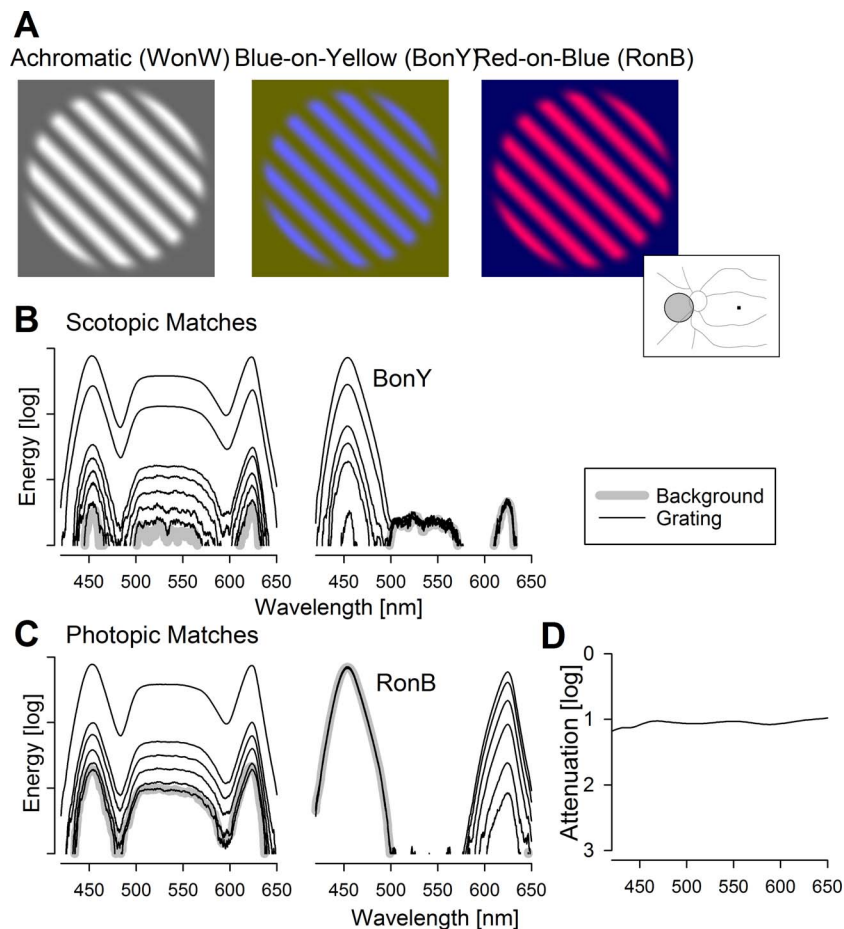
FIGURE 2. Achromatic and chromatic grating stimuli. (**A**) Appearance of the achromatic grating on achromatic background (white on white, WonW) and chromatic gratings on chromatic backgrounds (blue on yellow, BonY; and red on blue, RonB). *Inset right*, schematic of a left eye showing the optic nerve and major blood vessels. Fixation is to *dark square*, and *gray circle with black outline* shows the nasal localization of the gratings used. (**B, C**) Spectra showing the background (*thick gray lines*) and grating increments (*thin black lines*) for achromatic and chromatic stimuli. The backgrounds are matched in terms of scotopic luminance (**B**) or photopic luminance (**C**). All spectra are acquired under the same conditions and plotted on the same (relative) energy axis. (**D**) Absorption spectra of the 1 ND filter used to attenuate the stimuli.

Td) was estimated from phot-Td values and irradiance spectra[35] (Figs. 2B, 2C).

Whenever possible, the achromatic and chromatic gratings were tested in sets where the backgrounds were matched in terms of their effectiveness to stimulate a certain photoreceptor mechanism. For example, under scotopic conditions, WonW and BonY sets were tested with rod-matched backgrounds (Fig. 2B), whereas WonW and red-on-blue (RonB) sets were tested with L/M-cone–matched backgrounds (Fig. 2C). Testing was performed over a large range of adaptation conditions from −3 log scot-Td to 2.2 log phot-Td with the use of ND filters. The absorption spectra of the ND filters were near flat (Fig. 3D). For scotopic conditions, the necessity of stacking of multiple ND filters would be expected to cause some shifts at the spectral extremes, but such effects should be minimal for photopic conditions where fewer ND filters are stacked.

RESULTS

Eye Movements in Retinal Degenerations of Interest

The main impetus for the development of the modified MP1 was to design a potential outcome measure for treatments designed for two cohorts of patients: those with severe vision loss due to end-stage degeneration retina-wide and those with cone photoreceptor diseases. Both groups of patients show abnormal eye movements.[22,28,36] A representative example of retinal movements expected from end-stage retina-wide photoreceptor degeneration and "light perception" visual acuity was recorded from patient (P)5 (Fig. 3A), a 66-year-old patient with X-linked retinitis pigmentosa due to *RPGR* mutation. He would be a potential candidate for optogenetics therapy. In a dark room, the patient was instructed to gaze straight ahead, and eye movements were recorded directly from the retina under infrared illumination. There was small-amplitude nystagmus as well as a slow drift of the eyes in both *x* and *y* directions. Examples of retinal movements in cone photoreceptor diseases were recorded in P1, P2, and P3, representing patients with ACHM due to *CNGA3* or *CNGB3* mutations and BCM, respectively (Fig. 3A). All three patients would be potential candidates for gene augmentation therapy. In a dark room, the patients with cone diseases were instructed to fixate at a ~1° diameter target that was adjusted to be visible. In the two ACHM patients, eye movements had both horizontal and vertical components, whereas in the BCM patient most of the movement was along the horizontal meridian. There were periods of large saccades as well as
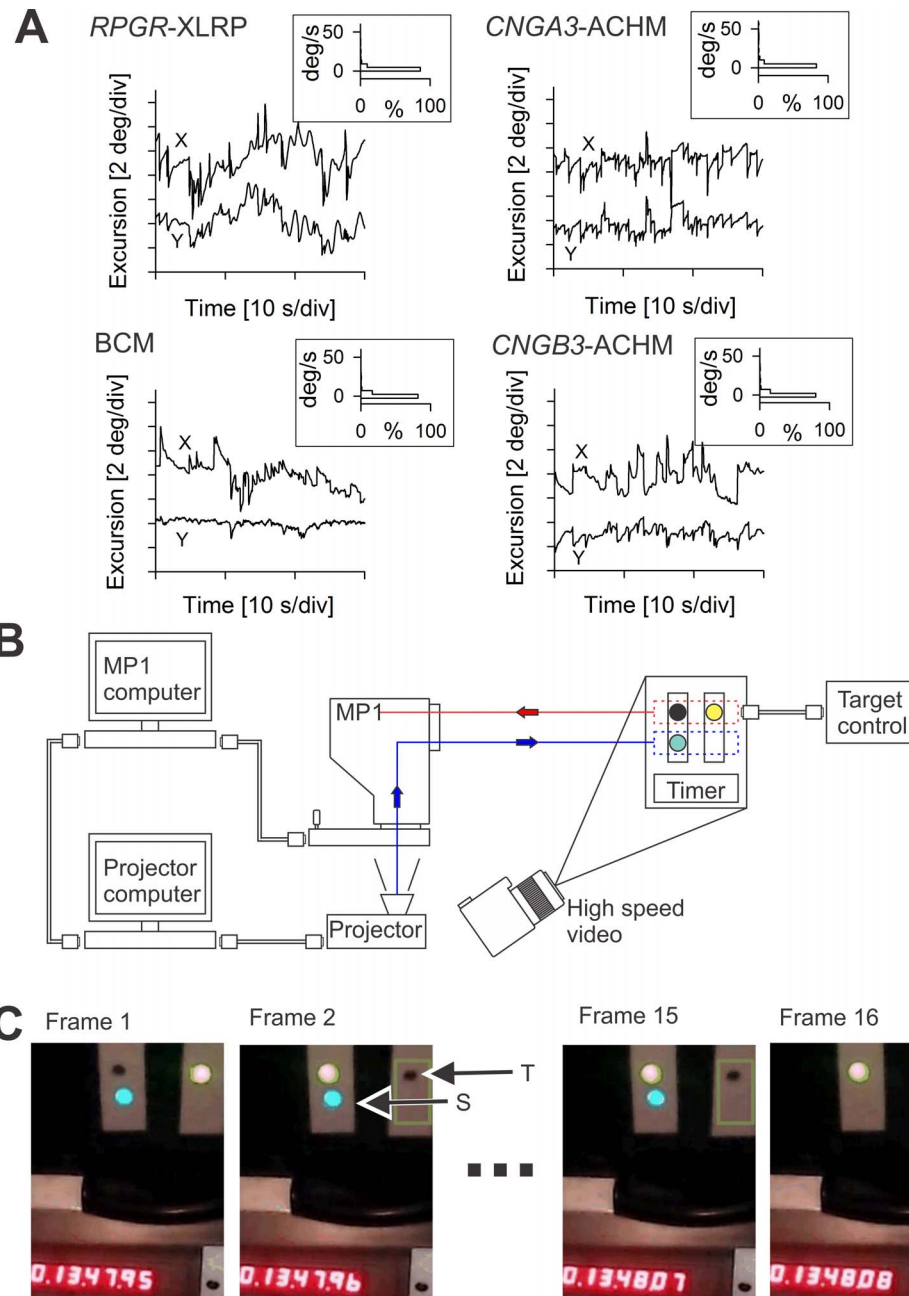
FIGURE 3. Expected eye movements and retinal tracking performance. (**A**) Eye movements of a 66-year-old *RPGR*-XLRP patient with end-stage retinal degeneration and light-perception visual acuity (*upper left*), a 26-year-old BCM patient with 20/100 visual acuity (*lower left*), a 13-year-old *CNGA3*-ACHM patient with 20/125 acuity (*upper right*), and an 18-year-old *CNGB3*-ACHM patient with 20/150 acuity (*lower right*). For each subject, eye movement data are shown as a chart recording for *x* and *y* directions (main images). During the recording, the XLRP patient was trying to hold the direction of his gaze without any visual cues in a dark room; the remaining patients, on the other hand, had a ∼1° diameter visible fixation target. The velocity of the eye movements was calculated and is shown as histograms (*insets*). (**B**) Schematic of the modified MP1 with its standard connection to the MP1 computer, which in turn is connected to an external projector computer that drives the projector coupled optically into the light path of the MP1. Also shown is the experimental system of a target, stimulus, and timer setup to measure the maximum time delay involved between tracking the target and displaying a stimulus at the correct spatial location. In this experimental system, a high-speed camera images the temporal sequence of the alternating target and the resulting stimulus movements. (**C**) First two and last two video frames from a representative sequence of 16 frames showing simultaneously the target (T) being tracked, the stimulus (S) that is driven by the modified MP1, and the 1/100-second timer. The video frames represent 1/120 second.

periods of relative stability. The estimated velocity of the eye movements varied in all four patients and could reach up to 100°/s; however, more than 84% of the samples had a velocity below 5°/s (Fig. 3A, insets). These examples illustrate the characteristics of the eye tracking needed for outcome measures in both types of patients.

Retinal Tracking and Stimulation Performance of the Modified MP1

We first evaluated static performance of the retinal tracking by measuring the detection linearity of a tracked object across the area of the modified MP1 that could be illuminated. For this

purpose, a trackable target was set up under external infrared (IR) illumination, and the modified MP1 was programmed to illuminate a small bright circular stimulus to overlay the target. In the worst-case scenario, static tracking error was found to be less than ~1°.

Important for stimulation of a fixed retinal locus in a moving eye is not only the static performance but also the dynamic performance of retinal tracking and stimulation system. The commercial unmodified MP1 system uses a video camera with 50-Hz interlaced fields to track the retinal movements over time and produces a stream of lateral shift information in horizontal and vertical directions every ~40 ms (corresponding to the 25-Hz frame rate), each with its own time stamp. We easily established that the external computer of the modified MP1 is able to read and process the stream of shifts without dropping any data by evaluating the consecutive time stamps of the samples. What is much more difficult to measure is the overall system delay associated with this stream of tracking data, that is, the delay between the time of the occurrence of a movement in the input and the resulting compensatory movement of the stimulus. The delay is not known for the standard MP1 or the modified MP1.

A system was set up whereby spatial changes in input and output could be simultaneously visualized using a high frame rate (120 fps) external video camera together with a high-resolution timer (Fig. 3B). The input to be tracked by the system was set up as two adjacent features: one darker than the background and one brighter than the background. The features could be electronically alternated, thus modeling an "instantaneous" saccade occurring faster than the frame rate of the MP1 imaging camera. The output was a small bright circular stimulus adjusted to fall immediately below the input target. The high-speed camera was placed such that the target, the light output, and a high-resolution timer could be simultaneously imaged. Figure 3C shows several frames from the high-speed recording. Frame 1 is immediately before the dark target is switched to the right side, whereas frame 2 (8.3 ms later) shows the dark target appearing. Frames 3 through 15 show no change, demonstrating the stimulus remaining on the left side. At frame 16 the stimulus moves to the right, suggesting a delay of 14 frames corresponding to 117 ms. Over several alternations, the mean time delay was 114 ± 15 ms ($n = 11$), corresponding to approximately three samples of the tracking information obtained at 25 Hz.

Next we estimated the proportion of this delay added by the modification as compared to the delay originating from the unmodified commercial MP1 system. For this measurement, the input was the same as described above, but the output was programmed by the commercial MP1 software to be a single Goldman V-sized stimulus presented on the internal LCD screen; the duration of the stimulus was set to the maximum allowed by the software (2000 ms) to permit a long enough time to record its movement in response to several feature switch cycles representing several saccades. The high-speed camera was set up to view the input, the output, and a timer simultaneously. Via frame-by-frame analysis, the time delay between the onset of the feature switch (saccade) and the corresponding onset of the stimulus movement was found to be 83 ± 12 ms ($n = 5$), corresponding to approximately two samples of the tracking information obtained at 25 Hz. Thus, we conclude that our modification adds 31 ms, on average, to the tracking delay. The dominant contributors to this additional delay are likely to be the transfer of information between the two computers as well as the transfer between the external computer and the DLP.

Spatial Resolving Properties of the Rod System

We used grating increments on dim backgrounds to evaluate spatial resolution of the peripheral rod system. The eyes were dark adapted, and the grating stimuli were expected to be visible to the normal rod system but below the threshold of the L/M- and S-cones in the periphery. Achromatic testing was performed with WonW and chromatic testing with BonY gratings. Two background luminances were used. The lower background level corresponded to −3 log scot-Td, which was achieved by the insertion of a total of 8 log ND filters in the light path and digital selection of either a W (R, G, B = 20, 20, 20) or a Y (R, G, B = 25, 25, 0) background. The spatial frequency of 0.6 cyc/deg first became perceptible with an increment of 0.7 log scot-Td. Greater increments above the background resulted in discrimination of finer spatial resolutions reaching 2.3 cyc/deg at 2.2 log scotopic increment (Fig. 4A, upper).

The higher background corresponded to −2 log scot-Td and was achieved with a total of 7 log ND filters inserted into the light path; the same set of achromatic and chromatic gratings/ backgrounds were used as for the lower background. White-on-white or BonY gratings of 0.8 cyc/deg first became perceptible with increments of 0.3 log scot-Td. Greater increments corresponded to visibility of higher spatial frequencies (Fig. 4A, lower). With the largest scotopic increment available (2.1 log scot-Td), spatial frequencies of 3.2 cyc/deg could be discriminated. Assuming peripheral cone thresholds to be near −2 log phot-Td, all BonY conditions and most WonW conditions would be expected to stimulate only the rod system.

Spatial Resolving Properties of the L/M-Cone System

To evaluate the spatial resolution of the peripheral L/M-cone system, we took advantage of light adaptation and longer wavelength gratings on shorter-wavelength backgrounds with the chromatic stimuli. Two backgrounds were used. The lower of the two backgrounds corresponded to −0.2 log phot-Td achieved by the insertion of a total of 5 log ND filters in the light path and either a W (R, G, B = 53, 53, 53) or a B (R, G, B = 0, 0, 255) background. WonW gratings of 2.1 cyc/deg first became perceptible with 0.1 log phot-Td increments (Fig. 4B, upper). With greater increments near 0.7 log phot-Td, both RonB and WonW gratings of 3.3 cyc/deg were reliably perceptible. With increments beyond 0.8 log phot-Td, all normal subjects could discriminate the 4.7 cyc/deg grating, which was the upper limit of the current system designed for low vision. The higher background corresponded to 2.2 log phot-Td achieved with a total of 3 log ND filters inserted into the light path. With increments of 0.1 log phot-Td, both the WonW and RonB gratings of up to 2.7 cyc/deg could be reliably discriminated (Fig. 4B, lower). With increments of 0.5 log phot-Td and beyond, most normal subjects could discriminate the 4.7 cyc/deg grating. Considering that the maximum available R grating on the B background corresponded to an increment of 0.1 log S-Td compared to 0.8 log phot-Td, it is likely that RonB gratings were detected by the L/M-cone system in normal eyes. Similarity of WonW results to those from RonB gratings suggest that the former are likely to be detected by the L/M-cone system also.

Spatial Resolving Properties of the S-Cone System

To evaluate the spatial resolution of the peripheral S-cone system, we took advantage of light adaptation (to saturate the rod system) and shorter-wavelength gratings (to preferentially
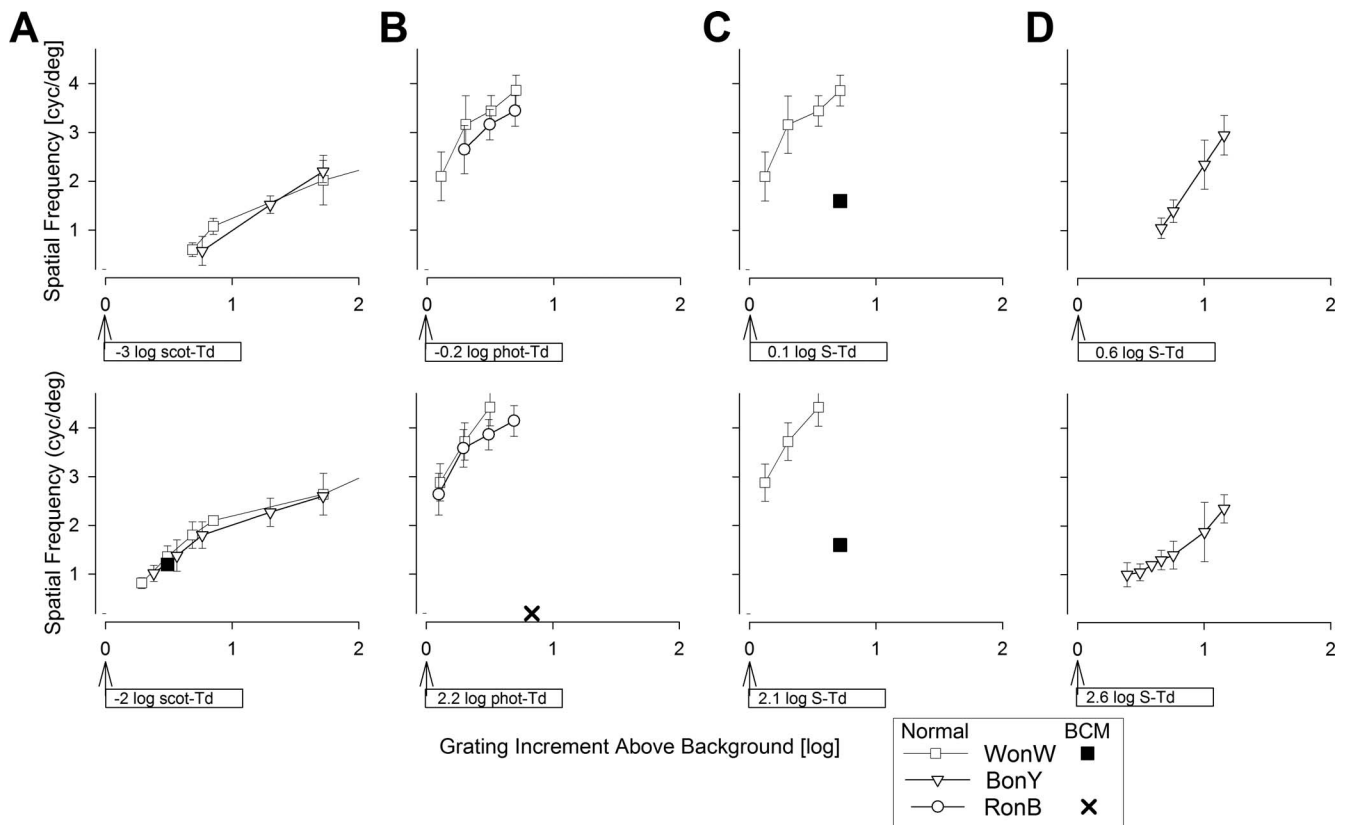
FIGURE 4. Spatial resolution under different adaptation conditions. (**A**) Dark-adapted eyes on −3 log scot-Td (*upper*) or on −2 log scot-Td (*lower*) W or Y backgrounds presented with WonW or BonY gratings of a range of scotopic increments. (**B**) Light-adapted eyes on −0.2 log phot-Td (*upper*) or on 2.2 log phot-Td (*lower*) W or B backgrounds presented with WonW or RonB gratings of a range of photopic increments. (**C**) Light-adapted eyes on 0.1 log S-Td (*upper*) or on 2.1 log S-Td (*lower*) W backgrounds presented with WonW gratings of a range of S increments. (**D**) Light-adapted eyes on 0.6 log S-Td (*upper*) or on 2.6 log S-Td (*lower*) Y backgrounds presented with BonY gratings of a range of S increments. *Symbols* show the discrimination of the direction of the highest spatial resolution grating under each grating/background condition. Results are from five normal subjects (*white symbols*) and one BCM patient (*black symbols*). The X in the lower image (**B**) represents the condition tested in the BCM patient who did not detect this RonB grating. *Error bars* are ±1 SD.

stimulate the S-cones) on middle- and longer-wavelength backgrounds (to reduce the increments available to the L/M-cones). Two Y backgrounds (R, G, B = 200, 200, 0) were used. The lower of the two backgrounds (0.6 log S-Td; 1.6 log phot-Td) was achieved by the insertion of a total of 5 log ND filters in the light path (Fig. 4D, upper) and the higher background (2.6 log S-Td; 3.6 log phot-Td) with 3 ND filters (Fig. 4D, lower). Discrimination of grating directions was not possible for increments less than 0.4 log S-Td at either background level. At 0.7 log S-Td increment with the lower background, and at 0.4 log S-Td increment with the higher background, 1 cyc/deg gratings could be discriminated. With greater increments, finer gratings were visible. These BonY conditions in the periphery under strong light adaptation likely represented the activity of S-cones considering that the maximum available B grating corresponded to an increment of 1.2 log S-Td as opposed to 0.02 log phot-Td.

Spatial Resolving Properties in Blue Cone Monochromacy

A 31-year-old BCM patient (P4) (Table) was evaluated with the modified MP1 to determine whether the combination of adapting conditions and chromatic gratings was able to discriminate between perceptions originating from different photoreceptor systems. The clinical, molecular, and retinal phenotype characteristics of the patient have been previously

published.[28,37] Blue cone monochromacy data were much more limited in scope compared to normal data. The dark-adapted BCM eye tested with a WonW achromatic grating at the −2 log scot-Td background showed results qualitatively similar to those of normal subjects (Fig. 4A, lower). Under strong B adaptation (2.2 log phot-Td), the BCM patient did not detect the highest available contrast (0.8 log phot; 0.1 log S) of chromatic RonB gratings and thus could not perform discrimination experiments (Fig. 4B, lower). Insensitivity to R stimuli was consistent with the severe abnormality of L/M-cone–driven vision in BCM.[28,37] Achromatic WonW gratings were visible to the BCM patient under light-adapted conditions (Fig. 4C). For both the lower (0.1 log S-Td; 0.2 log phot-Td) and the higher (2.1 log S-Td; 2.2 log phot-Td) achromatic backgrounds, the BCM patient could discriminate the direction of gratings up to 1.6 cyc/deg with 0.7 log S increments (Fig. 4C). These spatial frequencies were substantially lower than the results obtained in normals with the same conditions (Fig. 4C) but more similar to normal results obtained with BonY (Fig. 4D). These limited results in the BCM patient appear to confirm the conclusion that BonY recordings are driven by S-cones in normal subjects.

DISCUSSION

Perceptual testing is often performed under free-viewing conditions in which the subject either looks directly at the

target with his or her best vision (such as visual acuity testing) or looks at a fixation target while the stimulus is presented elsewhere within the visual field (such as computerized visual field testing). This approach often produces reliable, reproducible, and interpretable results as long as the subject has the ability to fixate steadily. On the other hand, there is much less certainty about the retinal location where perception is originating, and thus interpretation of the results, in patients who lack steady (foveal) fixation. For these patients, there is a long history of techniques used (variably named fundus perimetry, gaze-controlled perimetry, or microperimetry) coupling an objective estimate of the instantaneous gaze direction to the retinal location where the stimulus is being presented. Earlier approaches have involved operator judgment for the localization of retinal landmarks to adjust the location of the stimulus presentation (for examples, see Refs. 38–46). More modern systems image the retina with infrared illumination, detect the movement of the retina compared to a reference image, and present a stimulus adjusted to the movement of the retina (for examples, see Refs. 47–50). One of the modern systems is the Nidek MP1 microperimeter, which has been used in a large number studies since its introduction more than 10 years ago (examples include Refs. 47, 51–54). Modification of the hardware and the software has resulted in the scotopic version of MP1 primarily designed for dark-adapted two-color testing.[29,30] More recently, through a simple recalibration procedure, our group has performed "chromatic microperimetry" where spectrally opposing stimulus and background colors are used to preferentially probe different cone photoreceptor populations in cone diseases.[28] Here we report on a novel modification of the MP1 involving both hardware and software that allows the use of an external projector driven by an external computer as the source of light. Further work will be directed at choosing a succinct set of conditions tapping perception originating from different photoreceptor systems and defining the repeatability of the measurements in order to develop the feasibility experiments reported here into an outcome measure.

One of the key design features of the modified MP1 is the availability of high-luminance stimuli that may be necessary to activate optogenetic proteins. A clinical trial is currently under way (NCT02556736, Clinicaltrials.org) to introduce channelrhodopsins into retinal ganglion cells of patients with severe loss of vision and determine whether there is any evidence of improved vision. Assuming safety of the procedure, efficacy determination will require levels of retinal irradiance that will stimulate channelrhodopsin. The level of retinal irradiance that will be necessary in human eyes is currently unknown and is likely to be dependent on the expression level achieved. For any level of expression, it is thought that neural encoding of the stimuli will reduce the time-averaged retinal irradiance due to temporal sparsity of firing patterns applied at any given retinal location.[18] However, success of efficiently activating optogenetic proteins in nonphotoreceptor cells with encoded patterns requires availability of high peak retinal irradiance that can be precisely controlled in space and time in response to a retina that is dynamically and unpredictably moving. The modified MP1 presented here takes an important first step toward this goal. We designed the optics to provide a maximum retinal irradiance of approximately 0.1 mW.mm^{-2}, which is thought to fall within the bounds of retinal safety and potential effectiveness with first-generation optogenetic proteins.[18] For comparison, this maximal irradiance is approximately 4.3 log units higher than that available from the unmodified MP1, and approximately 2.8 log units higher than the standard (10,000 asb) stimulus available in many computerized perimeters.

The ability to repetitively stimulate the same region by tracking retinal features in a moving eye was an important prerequisite considered for choosing the MP1 as a starting platform. With the cooperation of the manufacturer, we were able to stream this retinal tracking information into an external computer and successfully use it to steer the stimuli presented by the external projector. However, there was an unavoidable delay between the retinal movement and the resulting stimulus movement. Two-thirds of the delay originated from the standard MP1, and one-third was added due to the modification. In eyes with stable fixation, the consequences of the delay are negligible. But in unstable eyes, the delay would be expected to result in errors between the intended and actual retinal locations to be stimulated, and the magnitude of the error would be proportional to the instantaneous velocity of eye movements. Based on data from patients who could be enrolled in relevant clinical trials, we conclude that the average absolute value of such errors is <0.25°, but the range can reach up to 4° with the current system. Future improvements in speed of image processing and data transfer are likely to reduce the delay and the magnitude of this error but could not eliminate it. For patients with "wandering" eye movements, but not for patients with repetitive fast saccades, predictive methods of retinal tracking could also be considered in the future to partially compensate for the system delay.

Changes in the instantaneous velocity of retinal movements coupled with a fixed tracking delay could be hypothesized to reduce the effective modulation depth of gratings by smearing the stimulus. However, previous work in idiopathic infantile nystagmus syndrome comparing tachistoscopic flashes to constant illumination has suggested that smearing of gratings has no consequence for visual acuity determinations.[55] Applicability of those results to ACHM and BCM patients remains unknown. To minimize the effects of smearing on perception in patients, we used a grating flash duration that was long compared to both the integration time of the underlying rod and/or cone photoreceptors and the typical duration of a saccadic "jerk" in patients with abnormal eye movements. Within the period of grating presentation, there were expected to be periods of eye movement with near-constant speed, which would correspond to a shift in retinal location stimulated (due to tracking delay) but no smearing when perception of highest spatial frequencies can occur.

An essential measure of human visual performance is spatial resolution. Most commonly, standard high-contrast letters under free-viewing conditions are used in bright ambient lights to evaluate the resolving power of the L/M-cone system. In cone photoreceptor diseases, however, rod (and sometimes S-cone) photoreceptors can dominate low levels of vision even in daytime conditions.[27,28,37] The overarching aim of gene therapies for cone photoreceptor diseases is to improve L/M-cone–driven visual performance of patients. However, it is hypothetically possible, maybe even likely, that early-phase gene therapies will result in incremental improvements at best, and the detection of such improvement within the context of the native vision of these patients will require specialized outcome measures. The modified MP1 developed here had the luminance and chromaticity range to be applicable as such a specialized outcome measure. Toward this aim, in preliminary experiments we measured grating visual acuities near the increment threshold in the nasal retina of normal subjects and a BCM patient. Under conditions where grating discrimination is likely to be dominated by the peripheral rod system, we found spatial frequencies of 1 cyc/deg near luminance increment thresholds representing peak sensitivity. Comparable were the limited results from the BCM patient and previous findings performed under similar but not identical conditions.[56-58] Red gratings on bright blue backgrounds were not

detectable by the BCM patient even at the highest contrast levels, consistent with the expected pathophysiology in BCM.[57,59,60] For these L/M-cone–mediated conditions, spatial frequencies of 2 to 3 cyc/deg were measured near peak sensitivity with our flashed stimuli in normal subjects; previously reported results in the periphery with drifting stimuli have been somewhat lower.[61] And finally, blue gratings on bright yellow backgrounds tapped perception originating from S-cones and showed spatial frequencies of 1 to 1.5 cyc/deg near peak sensitivity in the nasal periphery. Comparable results have been obtained from central S-cones near threshold[57,59,60] or implied by suprathreshold results in perifovea or periphery.[60,61]

In conclusion, the modified MP1 described here provides an early step with promising potential toward presenting varied stimuli of a very wide range of luminance and chromaticity with precise spatiotemporal control locked to retinal features.

Acknowledgments

References

1. Bramall AN, Wright AF, Jacobson SG, McInnes RR. The genomic, biochemical, and cellular responses of the retina in inherited photoreceptor degenerations and prospects for the treatment of these disorders. *Annu Rev Neurosci*. 2010;33: 441–472.

2. Ho AC, Humayun MS, Dorn JD, et al. Long-term results from an epiretinal prosthesis to restore sight to the blind. *Ophthalmology*. 2015;122:1547–1554.

3. Jacobson SG, Cideciyan AV. Treatment possibilities for retinitis pigmentosa. *N Engl J Med*. 2010;363:1669–1671.

4. Bi A, Cui J, Ma YP, et al. Ectopic expression of a microbial-type rhodopsin restores visual responses in mice with photoreceptor degeneration. *Neuron*. 2006;50:23–33.

5. Tomita H, Sugano E, Yawo H, et al. Restoration of visual response in aged dystrophic RCS rats using AAV-mediated channelopsin-2 gene transfer. *Invest Ophthalmol Vis Sci*. 2007;48:3821–3826.

6. Lagali PS, Balya D, Awatramani GB, et al. Light-activated channels targeted to ON bipolar cells restore visual function in retinal degeneration. *Nat Neurosci*. 2008;11:667–675.

7. Lin B, Koizumi A, Tanaka N, Panda S, Masland RH. Restoration of visual function in retinal degeneration mice by ectopic expression of melanopsin. *Proc Natl Acad Sci U S A*. 2008; 105:16009–16014.

8. Thyagarajan S, van Wyk M, Lehmann K, Löwel S, Feng G, Wässle H. Visual function in mice with photoreceptor degeneration and transgenic expression of channelrhodopsin 2 in ganglion cells. *J Neurosci*. 2010;30:8745–8758.

9. Doroudchi MM, Greenberg KP, Liu J, et al. Virally delivered channelrhodopsin-2 safely and effectively restores visual function in multiple mouse models of blindness. *Mol Ther*. 2011;19:1220–1229.

10. Nirenberg S, Pandarinath C. Retinal prosthetic strategy with the capacity to restore normal vision. *Proc Natl Acad Sci U S A*. 2012;109:15012–15017.

11. Cideciyan AV, Jacobson SG, Beltran WA, et al. Human retinal gene therapy for Leber congenital amaurosis shows advancing retinal degeneration despite enduring visual improvement. *Proc Natl Acad Sci U S A*. 2013;110:E517–E525.

12. Beltran WA, Cideciyan AV, Iwabea S, et al. Successful arrest of photoreceptor and vision loss expands the therapeutic window of retinal gene therapy to later stages of disease. *Proc Natl Acad Sci U S A*. 2015;112:E5844–E5853.

13. Zhang F, Prigge M, Beyrière F, et al. Red-shifted optogenetic excitation: a tool for fast neural control derived from Volvox carteri. *Nat Neurosci*. 2008;11:631–633.

14. Lin JY, Lin MZ, Steinbach P, Tsien RY. Characterization of engineered channelrhodopsin variants with improved properties and kinetics. *Biophys J*. 2009;96:1803–1814.

15. Loudin JD, Simanovskii DM, Vijayraghavan K, et al. Optoelectronic retinal prosthesis: system design and performance. *J Neural Eng*. 2007;4:S72–S84.

16. Grossman N, Poher V, Grubb MS, et al. Multi-site optical excitation using ChR2 and micro-LED array. *J Neural Eng*. 2010;7:16004.

17. Pandarinath C, Carlson ET, Nirenberg S. A system for optically controlling neural circuits with very high spatial and temporal resolution. *IEEE 13th International Conference on Bioinformatics and Bioengineering (BIBE)*. 2013;1–6.

18. Yan B, Vakulenko M, Min SH, Hauswirth WW, Nirenberg S. Maintaining ocular safety with light exposure, focusing on devices for optogenetic stimulation. *Vision Res*. 2016;24:57–71.

19. Fine I, Boynton GM. Pulse trains to percepts: the challenge of creating a perceptually intelligible world with sight recovery technologies. *Philos Trans R Soc Lond B Biol Sci*. 2015;370: 20140208.

20. Leigh RJ, Zee DS. Eye movements of the blind. *Invest Ophthalmol Vis Sci*. 1980;19:328–331.

21. Hall EC, Gordon J, Hainline L, Abramov I, Engber K. Childhood visual experience affects adult voluntary ocular motor control. *Optom Vis Sci*. 2000;77:511–523.

22. Cideciyan AV, Aguirre GK, Jacobson SG, et al. Pseudo-fovea formation after gene therapy for RPE65-LCA. *Invest Ophthalmol Vis Sci*. 2015;56:526–537.

23. Ivanova E, Hwang GS, Pan ZH, Troilo D. Evaluation of AAV-mediated expression of Chop2-GFP in the marmoset retina. *Invest Ophthalmol Vis Sci*. 2010;51:5288–5296.

24. Yin L, Greenberg K, Hunter JJ, et al. Intravitreal injection of AAV2 transduces macaque inner retina. *Invest Ophthalmol Vis Sci*. 2011;52:2775–2783.

25. Werblin F, Palanker D. Restoring vision to the blind: advancements in vision aids for the visually impaired. *Trans Vis Sci Technol*. 2014;3(7):9.

26. Buck SL, Knight R. Partial additivity of rod signals with M- and L-cone signals in increment detection. *Vision Res*. 1994;34: 2537–2545.

27. Zelinger L, Cideciyan AV, Kohl S, et al. Genetics and disease expression in the CNGA3 form of achromatopsia: steps on the path to gene therapy. *Ophthalmology*. 2015;122:997–1007.

28. Luo X, Cideciyan AV, Iannaccone A, et al. Blue cone monochromacy: visual function and efficacy outcome measures for clinical trials. *PLoS One*. 2015;10:e0125700.

29. Crossland MD, Luong VA, Rubin GS, Fitzke FW. Retinal specific measurement of dark-adapted visual function: validation of a modified microperimeter. *BMC Ophthalmol*. 2011;11:5.

30. Birch DG, Wen Y, Locke K, Hood DC. Rod sensitivity, cone sensitivity, and photoreceptor layer thickness in retinal degenerative diseases. *Invest Ophthalmol Vis Sci*. 2011;52: 7141–7147.

31. Delori FC, Webb RH, Sliney DH; American National Standards Institute. Maximum permissible exposures for ocular safety (ANSI 2000), with emphasis on ophthalmic devices. *J Opt Soc Am A Opt Image Sci Vis*. 2007;24:1250–1265.

32. Judd DB. Report of U.S. Secretariat Committee on Colorimetry and Artificial Daylight. In: *Proceedings of the Twelfth Session of the CIE, Stockholm*. Vol. 1, pp. 11. Paris: Bureau Central de la CIE; 1951.

33. Vos JJ. Colorimetric and photometric properties of a 2-deg fundamental observer. *Color Res Appl*. 1978;3:125–128.

34. Nygaard RW, Frumkes TE. Calibration of the retinal illuminance provided by Maxwellian views. *Vision Res*. 1982;22: 433–434.

35. Miyahara E, Smith VC, Pokorny J. How surrounds affect chromaticity discrimination. *J Opt Soc Am A*. 1993;10:545–553.

36. Gottlob I, Proudlock FA. Aetiology of infantile nystagmus. *Curr Opin Neurol*. 2014;27:83–91.

37. Cideciyan AV, Hufnagel RB, Carroll J, et al. Human cone visual pigment deletions spare sufficient photoreceptors to warrant gene therapy. *Hum Gene Ther*. 2013;24:993–1006.

38. Kani K, Ogita Y. Fundus controlled perimetry: the relation between the position of a lesion in the fundus and in the visual field. *Doc Ophthalmol Proc Ser*. 1979;19:341–358.

39. Ohta Y, Miyamoto T, Harasawa K. Experimental fundus photo perimeter and its application. *Doc Ophthalmol Proc Ser*. 1978; 19:351–358.

40. Timberlake GT, Mainster MA, Webb RH, Hughes GW, Trempe CL. Retinal localization of scotomata by scanning laser ophthalmoscopy. *Invest Ophthalmol Vis Sci*. 1982;22:91–97.

41. Jacobson SG, Sandberg MA, Berson EL. Static fundus perimetry in amblyopia: comparison with juvenile macular degeneration. In: Greve EL, Heijl A, eds. *Fifth International Visual Field Symposium*. The Hague, The Netherlands: Dr. W. Junk Publishers; 1983:421–427.

42. Sunness JS, Johnson MA, Massof RW, Kays DL. Wilmer fundus camera stimulator. *Appl Opt*. 1987;26:1487–1491.

43. Borruat F-X, Jacobson SG. Advanced retinitis pigmentosa: quantifying visual function. In: LaVail, MM, Anderson RE, Hollyfield JG, eds. *Inherited and Environmentally Induced Retinal Degenerations*. New York: Alan R. Liss, Inc., 1989:3–17.

44. Jacobson SG, Borruat FX, Apáthy PP. Patterns of rod and cone dysfunction in Bardet-Biedl syndrome. *Am J Ophthalmol*. 1990;109:676–688.

45. Sunness JS, Schuchard RA, Shen N, Rubin GS, Dagnelie G, Haselwood DM. Landmark-driven fundus perimetry using the scanning laser ophthalmoscope. *Invest Ophthalmol Vis Sci*. 1995;36:1863–1874.

46. Szlyk JP, Paliga J, Seiple W, Rabb MF. Comprehensive functional vision assessment of patients with North Carolina macular dystrophy (MCDR1). *Retina*. 2005;25:489–497.

47. Midena E, Radin PP, Pilotto E, Ghirlando A, Convento E, Varano M. Fixation pattern and macular sensitivity in eyes with subfoveal choroidal neovascularization secondary to age-related macular degeneration. A microperimetry study. *Semin Ophthalmol*. 2004;19:55–61.

48. Rohrschneider K, Bültmann S, Springer C. Use of fundus perimetry (microperimetry) to quantify macular sensitivity. *Prog Retin Eye Res*. 2008;27:536–548.

49. Anastasakis A, McAnany JJ, Fishman GA, Seiple WH. Clinical value, normative retinal sensitivity values, and intrasession repeatability using a combined spectral domain optical coherence tomography/scanning laser ophthalmoscope microperimeter. *Eye (Lond)*. 2011;25:245–251.

50. Battu R, Khanna A, Hegde B, Berendschot TT, Grover S, Schouten JS. Correlation of structure and function of the macula in patients with retinitis pigmentosa. *Eye (Lond)*. 2015;29:895–901.

51. Midena E, Vujosevic S, Convento E, Manfrè A, Cavarzeran F, Pilotto E. Microperimetry and fundus autofluorescence in patients with early age-related macular degeneration. *Br J Ophthalmol*. 2007;91:1499–1503.

52. Cideciyan AV, Hauswirth WW, Aleman TS, et al. Vision 1 year after gene therapy for Leber's congenital amaurosis. *N Engl J Med*. 2009;361:725–727.

53. Cideciyan AV, Swider M, Aleman TS, et al. Macular function in macular degenerations: repeatability of microperimetry as a potential outcome measure for ABCA4-associated retinopathy trials. *Invest Ophthalmol Vis Sci*. 2012;53:841–852.

54. Strauss RW, Ho A, Muñoz B, et al.; Progression of Stargardt Disease Study Group. The Natural History of the Progression of Atrophy Secondary to Stargardt Disease (ProgStar) Studies: design and baseline characteristics: ProgStar Report No. 1. *Ophthalmology*. 2016;123:817–828.

55. Dunn MJ, Margrain TH, Woodhouse JM, Ennis FA, Harris CM, Erichsen JT. Grating visual acuity in infantile nystagmus in the absence of image motion. *Invest Ophthalmol Vis Sci*. 2014;55: 2682–2686.

56. Campbell FW, Robson JG. Application of Fourier analysis to the visibility of gratings. *J Physiol*. 1968;197:551–566.

57. Daw NW, Enoch JM. Contrast sensitivity, Westheimer function and Stiles-Crawford effect in a blue cone monochromat. *Vision Res*. 1973;13:1669–1680.

58. Hess RF, Nordby K. Spatial and temporal properties of human rod vision in the achromat. *J Physiol*. 1986;371:387–406.

59. Green DG. Visual acuity in the blue cone monochromat. *J. Physiol*. 1972;222:419–426.

60. Anderson SJ, Mullen KT, Hess RF. Human peripheral spatial resolution for achromatic and chromatic stimuli: limits imposed by optical and retinal factors. *J Physiol*. 1991;442: 47–64.

61. Greenstein VC, Zaidi Q, Hood DC, Spehar B, Cideciyan AV, Jacobson SG. The enhanced S cone syndrome: an analysis of receptoral and post-receptoral changes. *Vision Res*. 1996;36: 3711–3722.